Arabian Journal for Science and Engineering (2023) 48:4657–4673
https://doi.org/10.1007/s13369-022-07098-5

RESEARCH ARTICLE-CIVIL ENGINEERING

Numerical Modelling of Tunnels Excavated in Squeezing Ground Condition: A Case Study

Dipaloke Majumder[1] · M. N. Viladkar[1] · Mahendra Singh[1]

Received: 12 April 2022 / Accepted: 22 June 2022 / Published online: 10 August 2022

Abstract
Analysis and design of tunnels excavated in jointed rock mass is a challenging task. Situation aggravates when rock mass is found to experience a moderate or high squeezing. In this study, a novel numerical paradigm is presented for finite element analysis of tunnels excavated in squeezing ground. For this purpose, a tunnel model set is developed, namely Three Analysis Method (3AM). The 3AM involves three inter-connected models representing different tunnel construction stages. In this model, elastic–perfectly plastic behaviour of poor-quality rock mass is modelled by generalised Hoek–Brown criterion under biaxial in situ stress field. A case study of Maneri–Bhali Stage-I Hydro-electric Project (India) is investigated using this framework. Herein, tunnel support structure interaction responses are quantified in terms of tunnel convergence, stress components, ground-reaction curve, and support-characteristic curve. Results indicate that the 3AM is a realistic technique of tunnel simulation as it adopts the effect of tunnel convergence due to delay in support installation.

Keywords Squeezing ground · Tunnel excavation · Finite element modelling · Hoek–Brown criterion · Elasto-plastic analysis · Three Analysis Method

1 Introduction

Many underground construction activities are performed in the Himalayan region. In this region, geology is highly fragile and complex in nature due to presence of joints, fractures, folds, faults, shear zones, and other discontinuities. Magnitude of in situ stresses in the rock mass is very high thanks to extensive overburden and tectonic activities. As a result, upon creating a large size excavation, the rock mass experiences large convergence. On the other hand, excavation methodology, type of support systems of the underground cavity, and overall project cost are governed by the rock mass behaviour. Therefore, once the ground conditions are preliminarily estimated through a suitable ground condition prediction technique [1–5], detailed investigation becomes necessary at all problematic sections along the stretch of the tunnels.

In this study, squeezing phenomenon is defined as excessive tunnel convergence (elastic–perfectly plastic behaviour) that occurs upon excavation of tunnels and caverns as a consequence of particular conditions of four parameters, namely—(i) size of excavation, i.e., diameter (D) or width (B), (ii) height or depth of overburden (H), (iii) magnitude of in situ stresses (P_0), and (iv) quality of rock mass (i.e., Rock mass rating, *RMR* or Rock mass quality, Q or Geological strength index, *GSI*). Herein, the *RMR* is an index system for rock mass classification based on six geotechnical and geological parameters, like strength of intact rock, rock quality designation (RQD), spacing and conditions of discontinuities, groundwater condition, and joint orientation. Based on RMR values, the rock mass is divided into five classes such that- very good (RMR 100–81), good (80–61), fair (60–41), poor (40–21), and very poor (< 20) [6]. The Q- is another very sensitive index of rock quality and its value ranges from 0.001 to 1000. Use of the Q-system is specifically recommended for tunnels and caverns with an arched roof [6, 7]. The *GSI* is a widely used system of rock mass characterisation, developed to meet the need for reliable inputs related to rock mass properties required as input for numerical analysis

✉ Dipaloke Majumder
dipalokemajumder@gmail.com

M. N. Viladkar
mnviladkar50@gmail.com

Mahendra Singh
msingh.civil@gmail.com

[1] Civil Engineering Department, Indian Institute of Technology Roorkee, Roorkee 247667, India

or closed form (analytical) solutions for analysing tunnels, foundations, or slopes in rocks. The geological character of the rock, together with visual assessment of the mass it forms, is used as inputs for the selection of parameters for estimating rock mass strength and deformability. Consequently, this approach enables a rock mass to be considered as a mechanical continuum without losing the effect that geology has on its mechanical properties. Besides, it provides a field method for characterising difficult-to-describe rock masses. A chart is available in the literature for predicting GSI of different types of rock mass where the values of GSI vary from 0 to 100 [8].

On the other hand, many researchers argued to treat the squeezing phenomenon as an elastic–viscoplastic (i.e., time-dependent) deformation of the rock mass [9–11]. However, several studies [12–19] are reported in the literature where the squeezing is treated by elastic–perfectly plastic (EPP) response for avoiding numerical complexities. Here, the total tunnel convergence that one obtains theoretically through elastic–viscoplastic analysis at time $t = \infty$, is assumed to be identical to the tunnel convergence that one obtains in the elastoplastic analysis (assumption). The only difference is that viscoplastic analysis gives the occurrence of this convergence as a function of time, t. Hence, in the present study, the time dependence of squeezing has been neglected for the sake of simplicity.

For any numerical analysis of rock mass, it is essential to consider certain constitutive laws which reflect the yielding behaviour of rock mass appropriately. One of the most celebrated constitutive laws in rock engineering is perhaps the Hoek–Brown yield criterion (HBYC) [20, 21]. Several studies can be found in the literature which have employed this criterion for elasto-plastic (EP) or viscoplastic analysis of tunnel cavities [22, 23]. Pan et al. [24, 25] employed this criterion for elastic–viscoplastic analysis of tunnels in plane-strain condition and coal mine cavities in 3D condition using finite element method (FEM). However, yield surface of HBYC resembles a cone whose normal section in the octahedral plane is an irregular hexagon with sharp corners [26]. Hence, analogous to the Mohr–Coulomb yield criterion, the curse of singularity at the corners and apex of HBYC surface persists during the numerical analysis.

Few research workers [27, 28] have tried to solve the problem of singularity by rounding-off or by smoothening the failure surface at those critical locations. A few commercial software packages, like Phase^2 and PLAXIS have also incorporated this HBYC into their material library by considering the rounding-off of corners and the apex of yield/failure surface [29–32]. Few investigators have even approximated the HBYC by substituting Drucker-Prager criterion at corners and apex points of HBYC failure surface [33–36]. Although these approximating techniques at corners and the apex of failure surfaces are widely used in practice, the response generated through these approximate yield criteria does not converge to the exact solutions [37]. In order to address these issues, research workers [38] are now leaning more towards advanced numerical techniques for finite element (FE) implementation of HBYC for elasto-plastic analysis of tunnels in rock masses in which no smoothening or replacing the yield criterion at corners/edges is required. For instance, Kumar and Mohapatra [39] have presented lower-bound FE limit analysis formulation for HBYC in 2D by utilising semi-definite programming in conjunction with the conic optimisation. Karaoulanis and Chatzigogos [40, 41] have tried to solve this issue based on the spectral representation of stresses and strains for infinitesimal deformation plasticity coupled with return mapping scheme in principal stress directions. However, large displacements and finite strains were not considered in these studies. Its application to practical field problems is therefore somewhat limited. Modlhammer [42] suggested a numerical technique (namely four analysis method) to investigate the aspect of sequential construction of tunnels using the Mohr–Coulomb yield criterion in ABAQUS. Here, due to inherent limitation of ABAQUS, four separate FE models were implemented to replicate the construction delay during analysis. However, application of this technique is limited in squeezing tunnel problems due to high plasticity around tunnel cavity. Chortis and Kavvadas [43] investigated the characteristics of a tunnel junction construction in ABAQUS, where another tunnel intersected an existing main tunnel (+ shaped). Wu et al. [44] developed a damage evolution model in terms of volumetric strain depending upon the relationship among evolving permeability, porosity and volumetric strain. Here, the constitutive law in association with damage evolution model, was implemented in ABAQUS through an inbuilt 'user-subroutine to redefine field variables at a material point' (USDFLD) to analyse four diversion tunnels of a hydroelectric project. In this context, the studies of Clausen and Damkilde [37, 45] need to be mentioned where the return mapping scheme was used for the elasto-plastic FE formulation of HBYC with finite strains. However, application of this methodology into macro-scale elasto-plastic analysis of tunnels in poor quality rock masses is rarely found in the literature.

It is quite clear from review of earlier work that none of the methods developed for the analysis of tunnels has considered EP analysis of realistic tunnel models using FE formulation of actual HBYC. While some methods suffer from the curse of singularity, the others are not suitable for problems having high nonlinearity of the material response. In few studies, researchers have tried to overcome these issues by either smoothening or by rounding-off or by replacing the corner points of HBYC surface by other criteria. However, these noble efforts did not lead to exact solutions. Few three-dimensional studies [43, 46–49] were also undertaken, yet

these studies proved to be either too complicated or computationally expensive and hence unsuitable for use in practice.

In this paper, therefore, a novel framework has been presented for EPP analysis of tunnels excavated in a poor-quality rock mass using FE formulation of the actual HBYC [45]. In this framework, a tunnel model set has been developed, namely 'Three Analysis Method' (3AM). The 3AM involves three inter-connected models representing different tunnel construction stages. In this model set, EPP behaviour of poor-quality rock mass has been modelled by the generalised HBYC coupled with return mapping technique under biaxial in situ stress field. Finally, a case history of Maneri–Bhali Stage-I Hydro-electric Project (MB1HEP), India [50] is investigated using this framework.

2 Hoek–Brown Yield Criterion

In the present FE analysis, the tunnel is advancing through an isotropic-homogeneous rock mass. In the elasto-plastic analysis of this rock mass, the yielding behaviour is represented with nonlinear Hoek–Brown criterion [20], based on two basic parameters, namely uniaxial compressive strength of intact rock (σ_{ci}) and Hoek–Brown parameter (m_i), and two in situ parameters of jointed rock mass, namely GSI and disturbance factor (D'). The expression of the criterion is given in Eq. (1).

$$\sigma_1 = \sigma_3 + \sigma_{ci}\left(s + m_b\sigma_3/\sigma_{ci}\right)^a \tag{1}$$

where σ_1, σ_3 are effective major and minor principal stresses. The terms m_b,s and a are Hoek–Brown parameters of rock mass obtained from GSI, m_i and D' using Eqs. (2), (3) and (4), respectively.

$$m_b = m_i \exp\left[(GSI - 100)/\left(28 - 14D'\right)\right] \tag{2}$$

$$s = \exp\left[(GSI - 100)/\left(9 - 3D'\right)\right] \tag{3}$$

$$a = 0.5 + \left[\exp\left(-GSI/15\right) - \exp\left(-20/3\right)\right]/6 \tag{4}$$

During elasto-plastic deformations, once the rock mass has reached its yield limit, i.e., yield function, $f \geq 0$, updated stresses are computed by return mapping technique in conjunction with Newton–Raphson iteration at time, $t = \infty$ (approximately). The return mapping technique (predictor—corrector algorithm) employed in the present study is adopted from literature [37, 45]. Finally, the exact HBYC coupled with return mapping and large strain are implemented in the form of a user-defined material (UMAT) subroutine in FORTRAN 77 [51, 52].

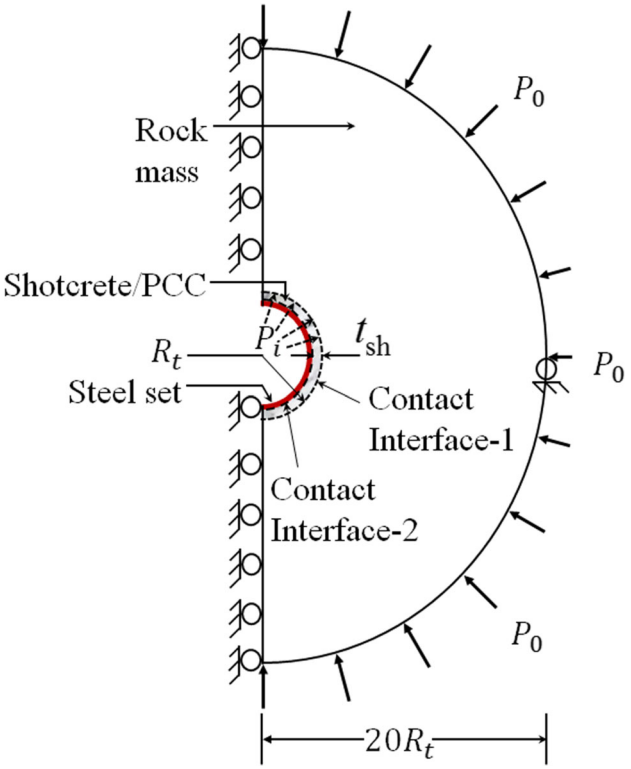

Fig. 1 Schematic diagram of FE model of tunnel cross-section with support systems assuming vertical symmetry (R_t = radius of excavated tunnel cavity, t_{sh} = thickness of PCC lining)

3 Finite Element Modelling

A 2D plane strain half-symmetric FE model of tunnel section exhibiting high squeezing is developed for numerical analysis in ABAQUS [52], as illustrated in Fig. 1. The tunnel excavation is simplified to a full-face excavation process. The FE tunnel consists of three parts, viz. rock mass surrounding the tunnel cavity, steel sets as a major support to the tunnel cavity, and plain cement concrete (PCC) lining as a primary support placed between rock mass and the steel sets.

3.1 Rock Mass Modelling

Rock mass section is modelled as a solid, homogeneous, isotropic plane strain continuum (Fig. 2). Eight–node biquadratic plane strain quadrilateral elements with reduced integration (CPE8R) are employed to mesh this part. Finer mesh is generated along the tunnel periphery to monitor the plasticity of rock mass. Since, the elasto-plastic response of rock mass is highly mesh dependent, a mesh sensitivity analysis is carried out to find the optimum number of elements for meshing in the present study, discussed later in Sect. 5.1. Herein, the constitutive behaviour of rock mass is adopted using the HBYC, already discussed in Sect. 2.

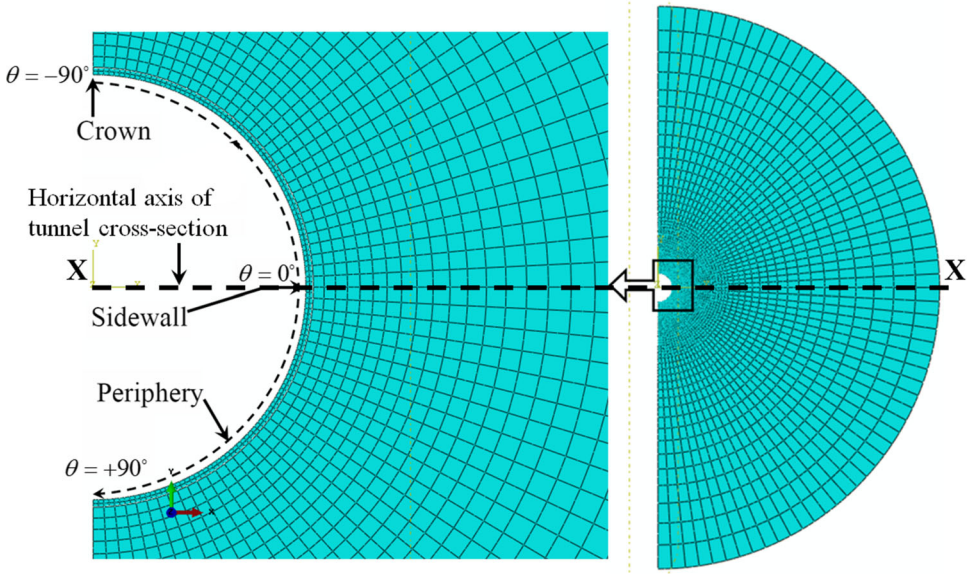

Fig. 2 Meshing of rock mass around tunnel cavity

3.2 Tunnel Support Elements

PCC lining is also modelled as a solid, homogeneous, isotropic continuum with CPE8R. Material behaviour of the PCC is modelled using the 'concrete damage plasticity model' (CDP) [53, 54] to capture the effect of yielding of lining materials. Here, the Young's modulus of concrete is calculated from $E_{\text{conc}} = 5000\sqrt{f_{ck}}$ [55]; where f_{ck} denotes the characteristics cube strength of concrete in N/mm^2. Appropriate parameters needed for the CDP model adopted from literature [56, 57], are given in Table 1. Further in CDP model, the phenomenon of tensile cracking and compressive crushing are assumed as the failure mechanisms of concrete material. Compressive response of PCC is defined through yield stress—inelastic strain curve of concrete whereas the tensile response is defined by yield stress—cracking strain curve (Table 1). The model also reflected the effect of damaged plasticity over the uniaxial tensile and compressive concrete response (Table 1).

Steel set support (I-section) is modelled as a wireframe and meshed with three-node quadratic beam element. Linear elastic response of steel set is defined by Young's modulus and Poisson's ratio of steel as 200 GPa and 0.3, respectively [56, 57]. The plastic response has been characterised by a yield stress–plastic strain curve of steel (Table 2).

3.3 Contact Modelling

Two contact interfaces are existing, viz., (i) contact interface-1: between PCC lining and rock mass, and (ii) contact interface-2: between steel sets and PCC lining (Fig. 1). A primary–secondary surface algorithm with Coulomb friction law is adopted to define these interfaces [52]. Frictional coefficient between rock mass and concrete is taken as $\mu = 0.65$ [58], and that between concrete and steel as 0.47 [59]. For achieving better convergence, 1 mm elastic slip is permitted, i.e., maximum transferable shear stress level is reached after a 1 mm displacement [42]. The normal behaviour along the interfaces is adopted such that penetration of interacting surface nodes can be avoided.

3.4 Boundary Conditions

Boundaries of the rock mass domain are placed far away from the cavity (i.e., 20 times R_t) so that stress–strain distributions around the tunnel remain unaffected. Herein, the boundary shape is chosen as circular (Fig. 1) so as to avoid unnecessary concentration of stresses at corners [19]. Along the left boundary of this FE model, vertical symmetry condition is applied to reduce the computational cost. The rightmost node of the rock mass is restricted to displace vertically to maintain the stability by assuming that variation of vertical stress is negligible due to large tunnel depth (deep tunnel condition).

3.5 Loading Conditions

The HRT tunnel is subjected to vertical (σ_V), and horizontal (σ_H) stresses to replicate the biaxial (non-uniform) in situ stress field. It is modelled by applying a pressure (P_0), normal to the circular rock mass boundary (Fig. 1). Here, P_0 is a function of resultant stress (traction) $\left(\sigma_R = \sqrt{\sigma_V^2 + \sigma_H^2}\right)$ multiplied with a factor (f_0), as shown in Eq. (5). The f_0 is obtained from an empirical field function (Eq. (6)) which is explicitly developed by combining coordinates of the circular periphery of rock mass domain and the variation of σ_V

Table 1 Various Parameters of concrete damaged plasticity model for M30 grade concrete [56, 57]

A. Compressive behaviour

Yield stress (MPa)	Inelastic strain	Damage parameter	Inelastic strain
9.0000	0.0000	0.0000	0.0000
22.5230	0.0001	0.0330	0.0001
29.0913	0.0004	0.1022	0.0004
29.4513	0.0009	0.1946	0.0009
27.5665	0.0013	0.2677	0.0013
25.1233	0.0018	0.3445	0.0018
22.5438	0.0022	0.4207	0.0022
20.0697	0.0026	0.4930	0.0026
17.8147	0.0030	0.5590	0.0030
15.8159	0.0034	0.6179	0.0034
14.0703	0.0038	0.6695	0.0038
12.5567	0.0042	0.7140	0.0042
11.2476	0.0045	0.7522	0.0045
10.1151	0.0049	0.7847	0.0049
9.1332	0.0053	0.8124	0.0053
8.2794	0.0056	0.8360	0.0056
7.5343	0.0060	0.8561	0.0060
6.8814	0.0063	0.8733	0.0063
6.3070	0.0066	0.8880	0.0066

B. Tensile behaviour

Yield stress (MPa)	Cracking strain	Damage parameter	Cracking strain
3.4507	0.0000	0.0000	0.0000
2.2957	0.0004	0.7401	0.0004
1.8840	0.0008	0.8681	0.0008
1.6516	0.0012	0.9164	0.0012
1.4961	0.0015	0.9407	0.0015
1.3821	0.0019	0.9550	0.0019

C. Other necessary Parameters

Density (MN/m^3)	0.0235
Dilation angle	36
Plastic potential eccentricity	0.1
Stress ratio	1.16
Shape of loading surface	0.6667
Viscosity parameter	0.003
Poisson's ratio	0.2

Table 2 List of elastoplastic properties of supporting steel sets and coefficients of friction for numerical modelling

A. Elastic properties of steel [66]

Young's modulus of steel (GPa)	200
Poisson's ratio of steel	0.3

B. Plastic properties of steel [56]

Yield stress (MPa)	Plastic strain
200.2	0
246	0.02353
294	0.0474
374	0.09354
437	0.1377
480	0.18

C. Coefficients of friction

Rock mass and concrete [58]	0.65
Concrete and steel [59]	0.47

and σ_H over the same. However, the shear component generated due to resultant traction of anisotropic far-field stress is neglected here.

$$P_0 = f_0 \cdot \sigma_R \tag{5}$$

$$f_0 = \frac{\left(\sigma_V \left|\frac{y}{20\,R_t}\right| + \sigma_H \left|\frac{x}{20\,R_t}\right|\right)}{\sqrt{\sigma_V^2 + \sigma_H^2}} \tag{6}$$

where x, y denote coordinates of rock mass, and R_t is tunnel radius. Here, the tunnel centre is located at coordinate (0, 0). In addition, the tunnel excavation process is simulated in this study by using the 'load reduction technique' [42] in which an internal pressure (P_i) is applied over the pre-existing tunnel periphery (Fig. 1) to simulate un-excavated ground. Herein, P_i is applied along the circular tunnel periphery using Eq. (7) where the factor f_i is calculated from Eq. (8), especially proposed to control the value of P_i replicating the biaxial effect of in situ stresses on the tunnel surface.

$$P_i = \sigma_H \cdot f_i \tag{7}$$

$$f_i = 1 + \frac{|y|}{R_t} \cdot \left(\frac{\sigma_V}{\sigma_H} - 1\right) \tag{8}$$

In this context, it may be noted that the in situ stresses in the rock mass surrounding a tunnel cavity are usually triaxial (or biaxial for plane strain condition) and compressive.

Besides, the shape of the yield (plastic) zone around the tunnel opening is primarily governed by the ratio of horizontal and vertical in situ stresses ($k = \sigma_H / \sigma_V$) and internal friction (ϕ°) of rock mass. These in situ stresses are generated due to static or gravity load of rock mass and tectonic activity. Thus, the effect of gravity is taken into account indirectly through in situ stresses in the present study. However, around the cavity, failure of broken rock mass within the plastic zone due to gravity has been neglected to retain the symmetry of the problem. In this context, several studies [19, 43, 60–62] can be mentioned where the above-mentioned approach were adopted.

3.6 Simulation of Rock Mass–Tunnel Support Interaction

In this study, a set of FE models are devised in-plane strain condition to simulate the rock mass surrounding a tunnel, combined support system, and their interaction with all the features mentioned in Sect. 3.1–3.5. The model set is developed to analyse tunnel support interaction considering pre-displacements and construction delay of combined support system (PCC lining and steel sets) with three distinct tunnel models interconnected in a series. Hence, it is termed as 'Three Analysis Method' (3AM). A schematic diagram of this tunnel support system is already provided in Fig. 1.

In comparison with the existing 'four analysis method' [42] and 'Abaqus example problem 1.1.11' [52], the proposed 3AM is not only a one-step simplification, but it also reduces the modelling efforts significantly, where an ample number of nodes are present on the tunnel periphery (see Sect. 3.5) to capture high plasticity of material. Functions of the three individual tunnel models used in this technique are –

(i) Model-A involves only the rock mass part with a circular outer boundary. It is developed to simulate the pre-displacements and initial support delay for finding the deformed coordinates (geometry) of tunnel periphery to model the PCC lining,
(ii) Model-B is built to find deformed coordinates along the internal periphery of PCC lining for modelling the steel sets, and
(iii) Model-C is developed for complete simulation of tunnel construction procedure with PCC lining and steel sets.

These three models are inter-connected so that the tunnel wall deformations obtained from Model-A are incorporated in Model-B. Then, deformations of PCC lining obtained from Model-B are incorporated in Model-C for final computation. In addition, it may be noted that at the time of defining FE simulation parameters, finite strain calculations have been adopted. Hence, the 'stress' indicates to the 'true' or 'Cauchy' stress (i.e., force per current area) while the 'strain' refers to the logarithmic strain values [63]. In ABAQUS program, the above approach is invoked by turning on 'NLgeom' option in 'Step Editor' module [52].

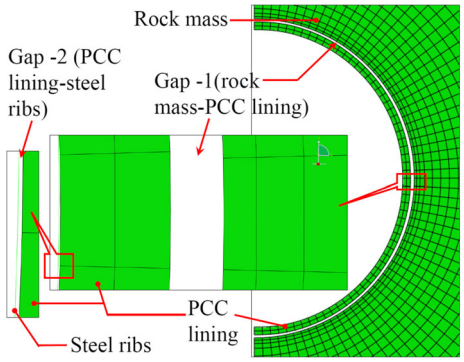

Fig. 3 Initial step of FE model in 'Three Analysis Method' with gaps between each part

3.6.1 Computational Steps

This section describes the computational steps of Model-C. Analogously, the Model-A and Model-B are executed; besides, few notes are provided within the following steps regarding the execution of those two tunnel models.

Step 0-Initial conditions: Simulation of Model-C begins with the assembly of all four parts, viz. rock mass with a cavity, PCC lining, and two portions of steel sets (upper portion and lower portion) in the initial step. However, there are gaps between rock mass and PCC lining and between PCC lining and steel sets (Fig. 3). Contact formulations are defined along interface-1 and interface-2, and boundary conditions are set. A tie joint is set up between the closest two nodes of the upper portion and lower portion of steel sets.
[*Initial step of Model-A and Model-B*: In Model-A, both the support systems are not present, whereas, in Model-B, the steel sets are absent. The corresponding contact interactions and boundary conditions are also absent in the initial steps of these models. Otherwise, all other conditions are the same as Model-C in these models.]
Step-1: Application of in situ stress: In this step, degrees of freedom, namely DOF 1 and DOF 2 are set to fixity along the tunnel periphery (Fig. 4a). In situ stress field (P_0) is applied over the rock mass boundary using Eq. (5). All support elements (PCC lining and two steel sets) and the corresponding contact interactions among these parts are deactivated.
[From Model-B, PCC lining and the corresponding contact interaction along the interface-1 are removed.]
Step-2: Application of internal pressure: In this step, DOF 1 and DOF 2 are set free along the tunnel periphery (Fig. 4b). Internal pressure (P_i) is applied along the tunnel periphery

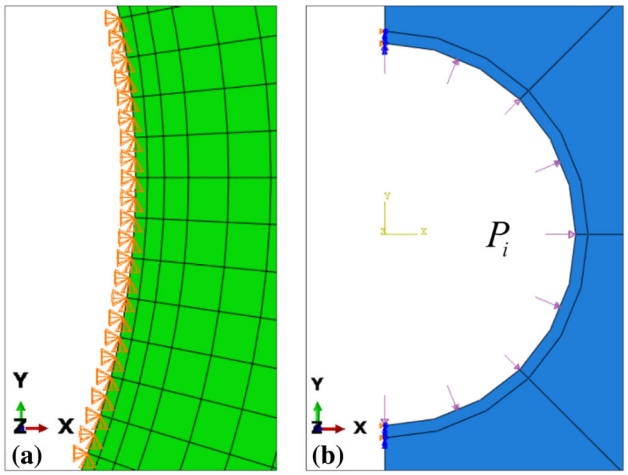

Fig. 4 **a** Fixing tunnel periphery at Step-1, and **b** applying internal pressure (P_i) in Step-2 in Three Analysis Method

using Eq. (7). At this point, load reduction factor (α_i) comes into play to control (reduce) the internal force amplitude in the subsequent steps; in step—2, $\alpha_i = 0\%$.

Step-3: Excavation begins: In this step, the tunnel cavity excavation is started by setting α_i to 0.20 (i.e., 20% of P_i). As a result, the rock mass deformed radially inwards as the simulation progressed.

[Obtain nodal coordinates for PCC lining (End of Model—A): On completion of Step- 3, the calculation terminates in Model-A, and the coordinates of displaced nodes along the tunnel periphery are recorded from the results for modelling PCC lining in Model-B.]

Step-4: Installation of PCC lining: PCC lining elements along with the contact interaction property between rock and PCC lining are reactivated in this step. Any penetration of interacting surface nodes (over-closure) is also corrected, if exist.

Step-5: Excavation resumes: As soon as the α_i increases beyond 0.30, the tunnel and rock mass together with PCC lining deformed radially inward. These deformations continued to grow until α_i reached 0.55 (i.e., 55% of P_i).

[Obtain nodal coordinates for Steel sets (End of Model-B): At the end of Step-5, the calculation terminates in Model-B, and hence, the coordinates of displaced nodes along the inside edge of PCC lining are noted down for modelling the steel sets in Model-C.]

Step-6: Installation of steel sets: The steel sets are reactivated in this step. Like Step-4, the contact interaction between PCC lining and steel sets is activated with over-closure correction.

Steps-7, 8 and 9: Completion of excavation: As all the parts become active in Step-6, the excavation is resumed again in Step-7, and it is completed through Step-8 and Step-9. P_i is reduced to zero gradually by increasing the value of α_i in three steps, viz. 0.75, 0.95 and 1.0. Dividing the P_i reduction process into steps is crucial; otherwise, convergence problems may arise due to various nonlinearities. Finally, the FE simulation of tunnel support interaction is completed, and the results are stored for further analysis.

Kindly note that the α_i values in the above discussion are given for illustrative purpose only. Figure 5 presents a flow chart of 3AM with all computational steps.

4 Case Study: Headrace Tunnel of Maneri–Bhali Stage–I Hydro-Electric Project

4.1 Topography and Geology along Head Race Tunnel

An 8.56-km-long headrace tunnel (HRT) of circular cross section having 4.75 m finished diameter was constructed in the MB1HEP [50]. The HRT stretches from Maneri where a barrage and an intake structure was constructed, to a place in the downstream of Uttarkashi where the powerhouse is located. Excavation of this tunnel was completed by using four headings, viz. one from upstream end at Maneri, two from intermediate adits at Heena and the fourth one from the downstream end at Tiloth near Uttarkashi (Fig. 6).

The HRT passes through rock masses of quartzite, quartzite interbedded with thin bands of slate, chlorite schists, phyllites, meta-basics, and the basic intrusive of Garhwal Himalayas [64]. Rock mass beddings are affected by the Maneri central thrust towards North-East and East of this project area at 4.5 km East from Maneri. Rock formations of South and South-West region belong to the Chandpur group. There is another thrust, known as the North Almora thrust at 12 km from South-West of Uttarkashi. It separates the rock formations of Garhwal and Chandpur groups [50]. Closely spaced joints, brecciation, and shearing joints even in quartzites exist in this lithological unit because of intense folds and faults created by heavy tectonic activities of this region. Geological features along longitudinal section of the HRT are shown in Fig. 6.

4.2 Tunnelling Problems: Squeezing Phenomenon

At the time of tunnelling, field engineers encountered the problems of water-in inrush, cavity formation, and support failure due to heavy squeezing conditions. In this paper, the authors have focused their attention on the squeezing around tunnel periphery. Due to severe squeezing of rock mass, tunnelling operations were disturbed between chainage 5250 m and 5550 m (Fig. 6). In this stretch, the tunnel crosses through partially wet and thinly foliated meta-basics. The height of overburden varies from 700 to 900 m along the tunnel axis.

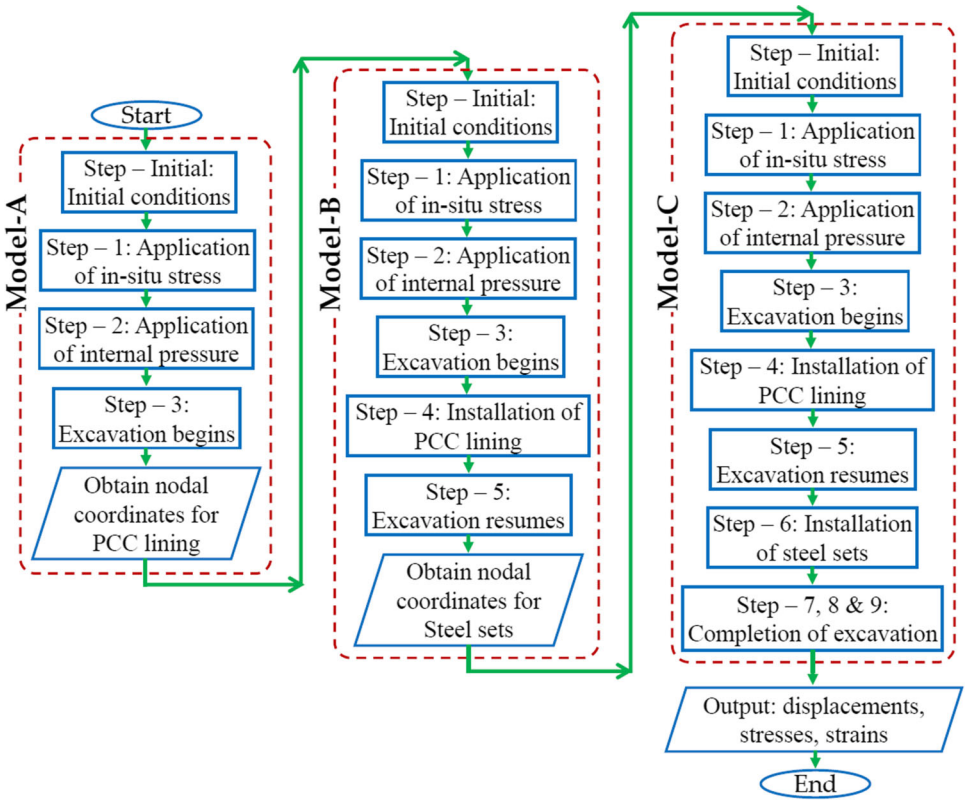

Fig. 5 Flow chart of all computational steps of proposed Three Analysis Method (3AM)

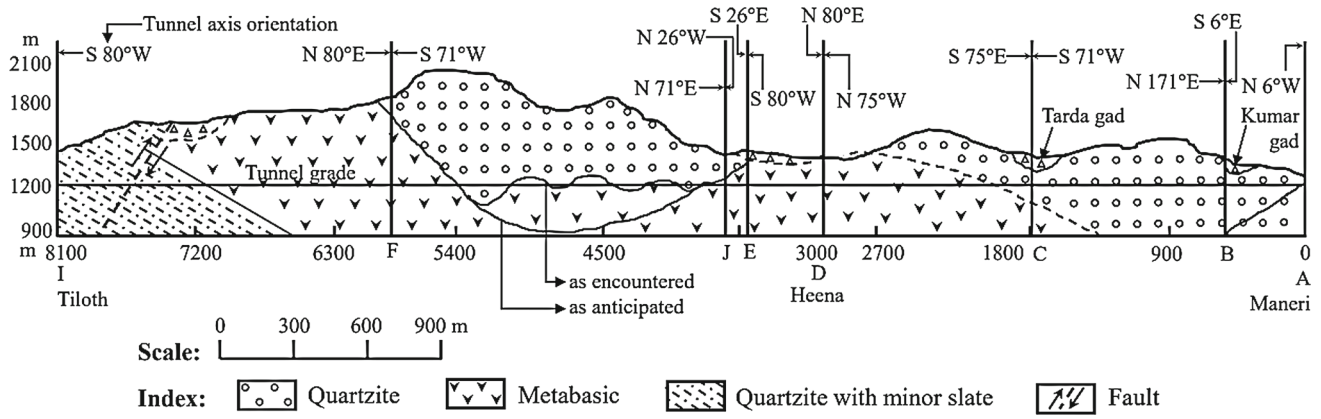

Fig. 6 Geological cross section along headrace-tunnel of Maneri–Bhali Stage-I Hydroelectric Project [50]

The tunnel was supported with ISMB 150 mm × 150 mm steel sets at 80 cm to 100 cm centre to centre (c/c) spacing [50]. The gap between the outer flanges of steel sets and the excavated rock surface was filled up with concrete mixture (Fig. 7). During excavation or supporting, no squeezing was experienced in this tunnel stretch. However, after 5–6 months, the squeezing behaviour of rock mass became visible as the backfilled concrete started cracking and the steel sets started deforming /buckling due to squeezing pressure.

Invert struts were therefore attached to each steel set of ISMB 150 mm × 75 mm in this stretch of the tunnel to restrict the buckling. Additionally, PCC was filled up to the inner flanges of steel sets. These remedial measures helped to control radial deformations temporarily. During the construction of final lining, it was noticed that the steel sets had deformed so much that their replacement became necessary to maintain the required finished diameter of tunnel. Even the floor of the tunnel had deformed by 800 mm. The twisted steel sets and the backfill concrete were subsequently removed, and the tunnel stretch was re-supported by ISMB 150 mm × 150 mm steel sets spaced at 75 cm c/c to obtain the required finished diameter.

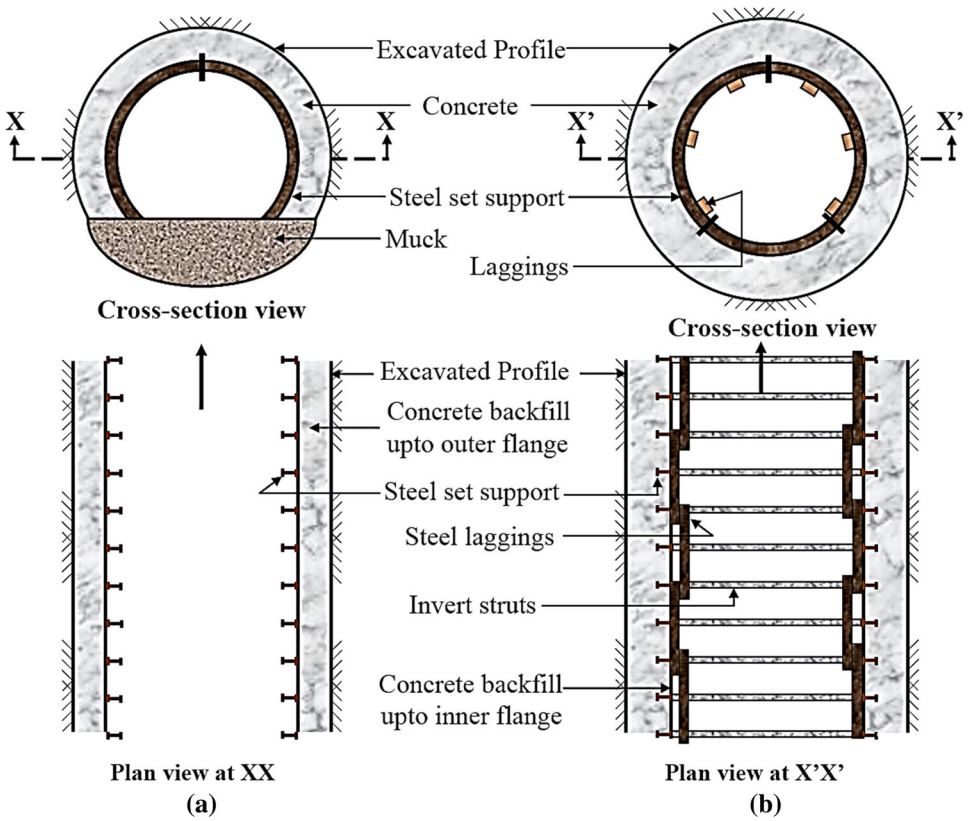

Fig. 7 Support systems adopted in squeezing ground condition [50]

Maximum tunnel closure observed was of the order of 8.9% of tunnel diameter in 600 days at the contact of meta-basics and quartzite, i.e., at a chainage of 5350 m. At another chainage of 5510 m in meta-basics, the total tunnel closure observed over a period of 100 days was about 2.18% where depth of overburden was 750 m. Different geological and geotechnical parameters corresponding to chainage 5350 m are listed below in Table 3.

5 Results and Discussion

In this analysis, the cross section of HRT at Chainage 5350 m of the MB1HEP is analysed using the proposed 3AM which is all a part of the Load Reduction Method. The responses of the HRT thus obtained is quantified in terms of tunnel convergence, development of stresses, and the plastic zone around tunnel periphery. In 3AM, both the aspects of delay in support installation and the sequential installation of different supports are considered. The response is also presented in terms of ground response curves (GRCs) of rock mass, and the support characteristic curves (SCCs) for the support systems. An attempt has also been made to compare the results obtained with the closed-form and other numerical solutions available in the literature.

During this analysis with 3AM, the values of load reduction factors, α_i (Sect. 3.6) are arrived at by conducting several trials. Every time, an attempt is made to equilibrate the maximum amount of in situ applied stress. The final values arrived at are $\alpha_2 = 0.30$ (i.e., 30%) and $\alpha_3 = 0.55$ (i.e., 55%). The analysis, therefore, considers that PCC lining (150 mm thickness of M30 grade) is applied after internal pressure reduction of 30% and the steel sets (ISMB 150 mm × 150 mm) are installed after an internal pressure reduction of 55%, respectively. In this context, it can be mentioned that the analysis is terminated when the applied internal pressure reduced to 87% of the applied in situ stress. The remaining 13% could not be equilibrated as the solution started diverging due to excessive distortion of elements along the tunnel periphery. At this stage, the total convergence of tunnel reached 10.22% corresponding to a radial displacement of 296.5 mm. Any attempt to further reduce the internally applied pressure leads to the collapse of the tunnel cavity. In reality, this tunnel collapsed after attaining the convergence of almost 9% [50]. Therefore, following discussion of results is presented essentially for the proposed 3AM.

5.1 Convergence Characteristics of Tunnel

Variation of percentage tunnel closure $\left(U/R_t \times 100\%\right)$ for the sidewall portion against normalised radial distance

Table 3 Rock mass properties along the HRT of Maneri–Bhali Stage–I HEP

Properties of rock mass	Symbol	Values
Chainage (m)	Ch.	5350
Rock type	-	Thinly laminated foliated, wet meta basics
Excavated tunnel radius (m)	R_t	2.4
Height of overburden (m)	H	800
Rock mass quality	Q	1.64–3.28
Geological strength index	GSI	39.57–40.92 (Avg. 40.5)
Modulus of deformation of rock mass (MPa)	$E_{\mathrm{d,rm}}$	8.08–10.72
Poisson's ratio of rock mass	ν	0.27
UCS of intact rock (MPa)	σ_{ci}	10
UCS of rock mass (MPa)	σ_{cm}	7.83
Hoek–Brown parameter of intact rock	m_i	7
Hoek–Brown parameters of rock mass	m_{b}	0.412
	s	0.00036
	a	0.511
Disturbance factor	D'	0.5
Vertical in situ stress (MPa)	σ_V	19.62
Horizontal in situ stress (MPa)	σ_H	13.73
Observed convergence (%)	–	8.9
Estimated ground conditions [2, 5]	–	Mild squeezing

(r/R_t), has been presented in Fig. 8a, and around the tunnel's opening in Fig. 8b. It may be noted that $\theta = 0^{\circ}$ corresponds to the sidewall portion, $\theta = -90^{\circ}$ coincides with the crown, and $\theta = +90^{\circ}$, with the tunnel invert. The convergence profile begins at 10.22% at tunnel periphery, and it reduces sharply with increasing r/R_t. Then, at a radial distance equal to 4.484 times R_t (= 13.00 m), the tunnel convergence has reduced to zero. Beyond this radius, the convergence is less than 0.5% (equivalent to about 14.5 mm of convergence). One can notice in Fig. 8b that the maximum convergence (10.22%) took place at the sidewall portion of tunnel, whereas the minimum convergence occurs at crown and invert portions. This is happening due to the failure of steel set joints and yielding of steel at sidewall region (further discussed in Sect. 5.5). This variation of convergence is a characteristic of biaxial in situ stress field around tunnel cavity.

A mesh sensitivity analysis is carried out to find the optimum number of mesh elements (as illustrated in Fig. 8c). Because the elasto-plastic characteristic is highly dependent on mesh size distribution. The total optimum number of elements chosen to be 3200 in the present study.

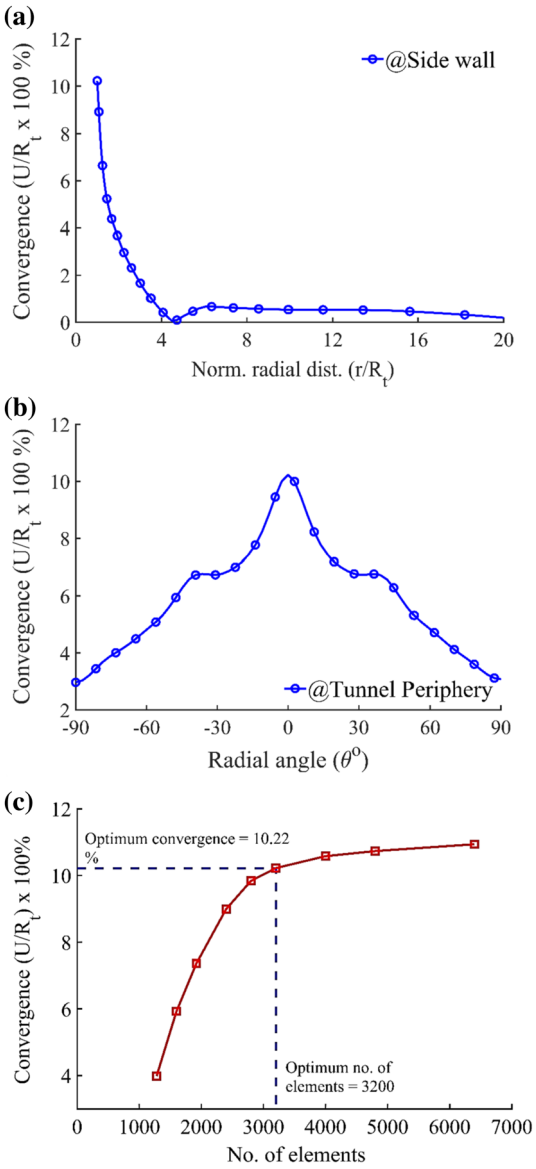

Fig. 8 Variation of tunnel convergence (%)-**a** in sidewall of tunnel, **b** around tunnel periphery and **c** with total no. of mesh elements in rock mass

Table 4 Comparison of computed results with field measured data

	Field measurement [50]	Computed from the present study
Tunnel closure (%) at chainage 5350 m	8.9	10.22

Further, the convergence obtained in the present analysis at Chainage of 5350 m has been compared with the corresponding values observed in field [50] as shown in Table 4. It can be seen that the computed convergence lies very close (less than 15%) to the observed convergence in the field.

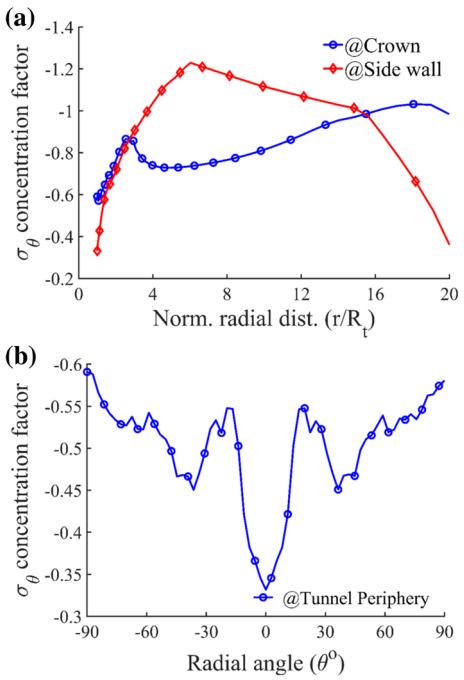

Fig. 9 Variation of σ_θ concentration factor at-**a** crown-sidewall and **b** around tunnel periphery. Radius of tunnel cavity, $R_t = 2.9$ m

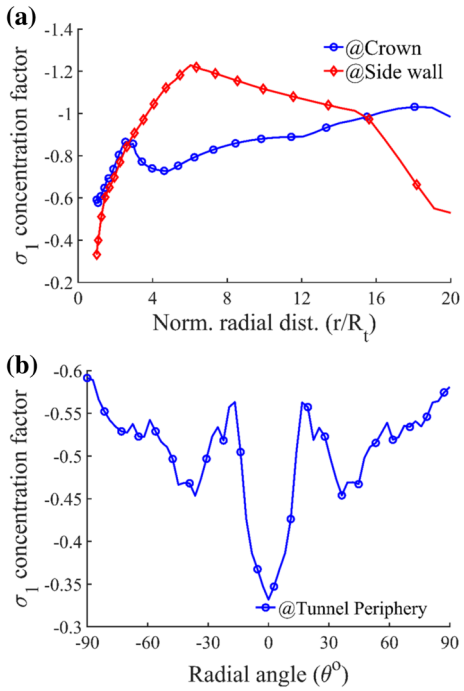

Fig. 10 Variation of σ_1 concentration factor at-**a** crown-sidewall and **b** around periphery of tunnel cavity

5.2 Variation of Tangential Stress

Variation of tangential stress (σ_θ) concentration factor (non-dimensional) is presented with respect to r/R_t in Fig. 9a for the crown and sidewall portion, and in Fig. 9b, with radial angle (θ°) around the tunnel periphery. The stress concentration factors have been calculated by dividing the values of σ_θ with the maximum value of resultant in-situ stress (traction) acting on the outer boundary (= 22.891 MPa).

The first profile (blue colour circle indices) in Fig. 9a shows that at crown portion σ_θ concentration is initially 0.58 (compressive) at $r/R_t = 1$, then it shoots up to 0.856 at $(r/R_t = 2.94)$. After that, it reduces 0.73 at $r/R_t = 4.58$, and then gradually increases to about 1.03 at a radial distance of about 18.05 times of R_t. This increase is due to the increase in strength of rock mass with a confining effect predominant near the boundary. The second σ_θ concentration profile (red colour diamond indices) in Fig. 9a, which has been plotted for the sidewall portion, shows that the maximum stress concentration factor being 1.23 (= 28.156 MPa, compressive) at a radial distance of about 6 times R_t (= 17.4 m). Beyond this distance, the σ_θ decreases continuously until it becomes equal to the applied in situ stress at the outer boundary. This peak point at 6 times R_t incidentally indicates the radius of the plastic zone developed around the tunnel periphery.

Figure 9b, displays the variation of σ_θ concentration factor around the tunnel periphery for the considered HRT section from MB1HEP. The plot shows that the proposed 3AM gives the maximum σ_θ concentration of 0.6 (= 13.73 MPa, compressive) which occurs at the crown ($\theta = -90^\circ$) and also at the tunnel invert ($\theta = +90^\circ$). Then, the concentration factor gradually reduces to ± 0.54 near the shoulder regions ($\theta = \pm 65^\circ$), and to about 0.33 at the sidewall ($\theta = 0^\circ$) portion. The magnitude of stress concentration is minimum at the sidewall because stresses have been mobilised due to rock mass deformations in this portion. On the other hand, the distribution of σ_θ concentration around the periphery is quite fluctuating due to rock mass–tunnel support interactions during tunnel construction in association with non-uniform in situ stresses.

5.3 Variation of Major Principal Stress

Variation of major principal stress (σ_1) concentration factors at points around the tunnel periphery has been plotted in Figs. 10. For a generalised biaxial state of in situ stress, Fig. 10a shows the variation of σ_1 concentration factor with r/R_t, and it suggests that σ_1 concentration factor in the crown region is 0.58 when 3AM is employed. The concentration factor shoots up to about 0.87 in rock mass at the vicinity of tunnel support system $(r/R_t = 2.54)$ as the rock mass is under confinement, then drops down to 0.725 at about $r/R_t = 5$ due to internal adjustments in rock mass. This curve follows the expected trend in compared to Fig. 9. Two kinks in the profile are due to the internal readjustment of rock mass, and stress level drops down in the zone where

rock mass is in a loosened state. The maximum value of σ_1 concentration factor attained in the rock mass is 1.03 at $r/R_t = 18.05$ from the tunnel periphery. The second profile (red colour diamond indices) in Fig. 10a shows the variation of σ_1 concentration factor in the sidewall portion of tunnel. The radius of plastic zone is about 6.04 times the tunnel radius, i.e., approximately 17.51 m $\left(r/R_t = 6.04\right)$. The stress at a distance of about 20 times of R_t, i.e., at the FE mesh boundary is equal to the applied in situ pressure.

Figure 10b displays the variation of σ_1 concentration around the tunnel periphery, for the considered tunnel section. This profile exhibits that maximum value of σ_1 concentration is about 0.59 (= 13.50 MPa, compressive) in the crown and invert portions, whereas it decreases to 0.45 (= 10.30 MPa) at $\theta = \pm 36.39°$. The minimum stress concentration occurs in the sidewall portion, the corresponding concentration factor in the rock mass being 0.33 (= 7.55 MPa).

5.4 Spread of Plastic Zone Around Tunnel Cavity

To estimate the spread of plastic zone or zone of broken rock mass around the tunnel cavity, plastic strain computation is necessary. However, in ABAQUS, the plastic strain (ε^p) in a material cannot be computed by built-in features when a user-defined material (UMAT) model is employed in the analysis. Therefore, ε^p is obtained indirectly by computing incremental plastic strain ($\Delta\varepsilon^p$) after each iteration within the UMAT subroutine by Eq. (9).

$$\Delta\bar{\boldsymbol{\varepsilon}}^p = \bar{\boldsymbol{D}}^{-1}\Delta\bar{\boldsymbol{\sigma}}^p \tag{9}$$

where $\bar{\cdot}$ denotes that the computations are carried out in principle stress space, e.g. $\bar{\boldsymbol{D}}$ consists of principle components of the elastic constitutive matrix ($\boldsymbol{D}$). The total equivalent plastic strain ($\tilde{\varepsilon}^p$) is then computed from Eq. (10) with the help of a state-dependent variable (SDV2) at each gauss point of the proposed FE model after each iteration.

$$\tilde{\varepsilon}^p = \tilde{\varepsilon}^p\big|_0 + \triangle\,\tilde{\varepsilon}^p = \tilde{\varepsilon}^p\big|_0 + \int_0^t \sqrt{\frac{2}{3}(\triangle\,\varepsilon^p : \triangle\,\varepsilon^p)}\,dt \tag{10}$$

Here $\tilde{\varepsilon}^p|_0$ is the initial equivalent plastic strain (generally zero or undefined) and the total time (fictitious) time used for analysis is given by t.

In this study, equivalent plastic strain in rock mass around the tunnel periphery has been found to be all tensile when the tunnel supports (PCC and steel sets) are installed. Magnitude of equivalent plastic strain in rock mass at crown and invert are 6.762% and, in the sidewall ($\theta = 0°$), it is 14.584% (see Table 5). The maximum tensile strain occurs in rock mass around the periphery at $\theta = \pm$ 67.7° and has a magnitude of 16.438%. Therefore, it is clear that even after providing the steel sets along with PCC lining, if the equivalent plastic tensile strains in rock mass around the periphery of the tunnel are so large, i.e., a variation from 6.762% at crown to 16.438% at θ = -67.7° to 14.584% in the sidewall (θ = 0°), then the tunnel has to collapse. This is what exactly happened, as stated in Sect. 4.3 that this mobilisation of strains took only 5–6 months and the tunnel collapsed along with complete yielding of steel sets (It may be noted that this analysis all the responses of rock mass around HRT are computed at time, $t = \infty$).

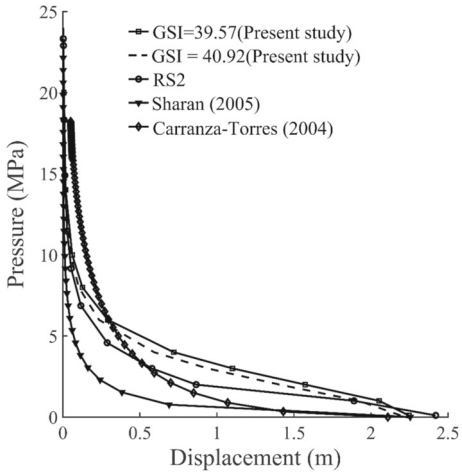

Fig. 11 Ground response curves at sidewall of tunnel under uniform in situ stresses for HRT section at Chainage 5350 m of MB1HEP

5.5 Ground Response Curves and Support Characteristics

5.5.1 GRC for Unsupported Tunnel

HereinIn this study, the GRCs have been computed by 'Load Reduction Method' in conjunction with an equivalent uniform external pressure of 22.9 MPa, which is the resultant (traction) of vertical ($\sigma_V = 19.62$ MPa) and horizontal ($\sigma_H = 11.772$ MPa) in situ stresses. For the present elasto-plastic analysis, GRCs of the unsupported tunnel section at chainage of 5350 m of the HRT (GSI = 39.57 and GSI = 40.92) from MB1HEP are plotted in Fig. 11. Here, the two GRCs correspond to the maximum and minimum values of GSI at that tunnel cross section. In these curves, a linear elastic part when the rock mass remains within the yield limit, followed by a nonlinear plastic part when the rock mass has yielded, is easily recognisable.

In Fig. 11, three more GRCs have been plotted for the HRT by using the analytical solutions of Sharan [60], Carranza-Torres [65], and the numerical solution obtained by using the commercial software, RS2. The final convergence and the

pattern of GRCs obtained through the present study have been found to be in good agreement with the solutions of Carranza-Torres and RS2. However, there are some differences with the closed-form solution presented by Sharan (2005) due to various assumptions and difference in the solution techniques. Therefore, it validates the overall strategy of elasto-plastic FE analysis of tunnels in squeezing ground condition considering the original form of generalised HBYC by using 3AM.

5.5.2 GRC and SCC for Supported Tunnel

Again, GRC and SCC are plotted for the selected HRT section in Fig. 12 after combined support installation using 3AM. Herein, the GRC represents an improved deformation profile of tunnel rock mass at sidewall point after the installation of PCC lining (150 mm thickness, M30 grade) and steel sets (ISMB 150 mm × 150 mm) under biaxial loading condition. Here again, an initial linear elastic part in the GRC, followed by a nonlinear-plastic part are prominently recognisable.

In Fig. 12, the two SCCs curves depicts the deformation profiles of PCC lining and steel sets under the action of present biaxial in situ stress level. Herein, the variation between the two SCCs of two support systems (PCC lining and the steel sets) shows a reasonable response during the simulation of 3AM as compared to the responses when the influence of tunnel rock mass displacement due to construction delay is neglected.

6 Summary of Results

Summary of various stress and convergence results, obtained—i) at steel sets, ii) at the interface between PCC inner wall and steel set outer wall, iii) at the interface between PCC outer wall and surrounding rock mass, is presented in Table 5. A glance at Table 5 suggests that equivalent plastic strain attained in steel sets is 8.715% (= 252.735 mm). Moreover, the radial stress (σ_r) and the major principal stress (σ_1) mobilised in steel sets are 362.92 MPa which is much larger than the yield stress of steel, usually taken as 250 MPa [66]. It indicates complete yielding of steel sets and the collapse of this tunnel even with an improved support system. The field observations also confirmed that this tunnel had collapsed. The numerical simulation using 3AM has therefore been validated.

6.1 Remarks

In Sect. 5.1–5.5, the failure behaviour or the collapse behaviour of a HRT section at chainage 5350 m from MB1HEP has been thoroughly investigated by the proposed FE modelling technique, i.e., 3AM. It comprised of three different but inter-related FE models. Herein, tunnel supports are not installed at the beginning of the analysis; instead, they are installed after a certain amount of excavation has been completed, i.e., PCC lining becomes active after 30% of internal pressure reduction, and steel sets become active only after internal pressure is reduced to 55%. Hence, installation of supports is sequential. Therefore, the displacement of the tunnel periphery due to the delay in installing tunnel supports has been incorporated in 3AM, making it a realistic model for simulating the tunnel construction procedure. The primary advantages of the proposed 3AM FE analysis procedure are as follows:

(i) Accurate geometrical modelling of each part (i.e., rock mass ground and different support elements) and defining appropriate boundaries became possible without any overlapping of different parts,
(ii) There is an ease of modelling contact interaction (i.e., Coulomb friction) among different parts,
(iii) The step of internal pressure determination under biaxial loading through an independent analysis is eliminated here. Hence, the analysis is simplified at least by one step, and thus, reduces the modelling effort significantly in comparison with the 'four analysis method' [42, 57]. Besides, formulation of used constitutive law (i.e., HBYC with return mapping at edges and corners in principal stress space) is accurate compared to commercially available software packages,
(iv) A constant thickness of support systems (i.e., PCC lining and steel sets) can be maintained during the simulation,
(v) Realistic behaviour of tunnel support interactive system can be determined in terms of tangential stresses of the support elements, and
(vi) Displacement (e.g. pre-displacements, support delay, combined support deformations) and stresses (e.g. tangential stress of PCC lining and steel sets) in support elements are determined with higher degree of accuracy and more reliability.

7 Conclusion

In this study, a novel numerical paradigm has been presented for the detailed analysis of tunnel case studies involving FE modelling of the squeezing tunnel sections. For this purpose, a set of FE models are developed in plane strain condition to simulate tunnel excavated in a rock mass with combined support systems and their interactions. The 3AM has been

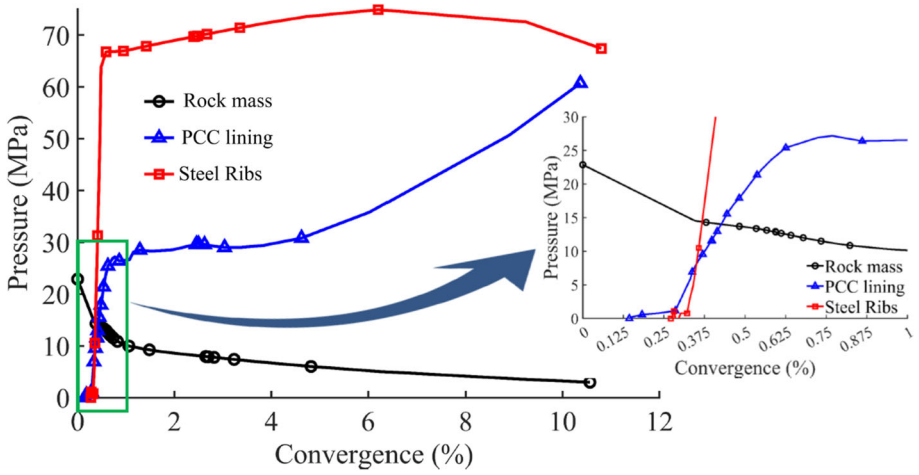

Fig. 12 GRC and SRC at sidewall point under biaxial in situ stresses for HRT section at Chainage 5350 m (MS1 = Model set-1 and 3AM = Three Analysis Method)

Table 5 Summary of results obtained via elasto-plastic analysis using Three Analysis Method for Maneri–Bhali Stage-I HEP

Locations	Steel Sets	PCC inner wall	PCC outer wall	Rock mass inner wall
Variables	At tunnel crown			
Convergence (%)	3.468	3.468	2.971	2.971
σ_r (MPa)	− 362.92	− 0.254	− 3.717	− 7.907
σ_θ (MPa)	–	− 79.024	− 54.365	− 13.532
$\sigma_{r\theta}$ (MPa)	–	− 0.275	− 0.054	0.042
σ_1 (MPa)	− 362.920	− 79.025	− 54.365	− 13.533
σ_3 (MPa)	–	− 0.253	− 3.717	− 7.907
Pressure (MPa)	120.970	45.199	32.838	11.650
$\widetilde{\varepsilon}^p$(%)	8.715	7.088	3.889	6.762
At tunnel sidewall				
Convergence (%)	10.532	10.797	10.224	10.224
σ_r (MPa)	− 202.210	− 0.034	− 0.824	− 3.724
σ_θ (MPa)	–	− 2.727	− 105.930	− 7.592
$\sigma_{r\theta}$ (MPa)	–	− 0.002	0.016	− 0.005
σ_1 (MPa)	− 202.210	− 3.541	− 105.940	− 7.592
σ_3 (MPa)	–	− 0.017	− 0.821	− 3.723
Pressure (MPa)	67.403	2.100	60.699	6.297
$\widetilde{\varepsilon}^p$(%)	1.198	2.182	9.923	14.584
Maximum values at tunnel periphery				
Convergence (%)	10.532	10.797	10.224	10.224
σ_r (MPa)	− 362.920	− 1.446	− 4.672	− 7.907
σ_θ (MPa)	–	− 79.024	− 105.930	− 13.532
$\sigma_{r\theta}$ (MPa)	–	− 8.558	− 8.137	− 1.292
σ_1 (MPa)	− 362.920	− 79.025	− 105.940	− 13.533
σ_3 (MPa)	–	− 0.537	− 4.407	− 7.907
Pressure (MPa)	120.970	45.199	60.699	11.650
$\widetilde{\varepsilon}^p$(%)	8.715	7.779	9.923	16.438

Note: (i) Negative sign indicates compressive stress; (ii) values at invert are the same as those at crown

developed considering pre-displacements and construction delay of combined support systems (PCC lining and steel sets) with three inter-connected FE models, viz. Model-A, Model-B, and Model-C. In these model set, material nonlinearity of all parts (i.e., rock mass ground, PCC lining, and steel sets) with appropriate contact interactions (Coulomb Friction law) among them is adopted. The response of rock mass is modelled using nonlinear Hoek–Brown criterion by employing the return mapping algorithm [45].

Once the numerical modelling part is completed, a critical tunnel section from MB1HEP is analysed using 3AM. The corresponding tunnel convergence and different stress components are presented along with equivalent plastic strains for the tunnel crown, sidewall, and around the tunnel periphery. Resulting convergence values have been validated with field observations as well as with solutions available in the literature. The GRCs and SRCs indicate that model set, 3AM, provides a realistic solution. Therefore, significant conclusions of the present study are listed below:

(i) An innovative FE modelling technique, namely 'Three Analysis Method', has been proposed for the numerical simulation of tunnel construction involving the excavation process and the installation of supports. Here, the pre-displacements of tunnel periphery and displacements due to support delay are considered using the Load Reduction Method.
(ii) Two empirical expressions, (5) and (7) have been developed for simulation of biaxial distribution of in situ stresses on the external circular boundary of rock mass domain in FE modelling and the corresponding internal pressure on the periphery of excavated tunnel surface, respectively.
(iii) One tunnel section from Maneri–Bhali Stage-I Hydroelectric project (India) has been investigated using the proposed paradigm. The responses of tunnel section are quantified in terms of tunnel convergence, various stress components, plastic strains, and GRCs and SRCs.

Finally, it can be stated that the present framework is one of the most comprehensive tools for the detail analysis of rock mass–tunnel support interaction in poor quality rock masses experiencing the squeezing ground condition. It is hoped that this knowledge would certainly help to handle other upcoming tunnelling projects in the problematic ground conditions of the lower Himalaya.

Acknowledgements The authors are thankful to Prof. Johan Clausen and Prof. Lars Damkilde from Alborg University, Denmark, Dr. Souvik Chakraborty from IIT Delhi, and Dr. Bibekananda Mandal from NIT Rourkela for their assistance and valuable suggestions.

Funding The authors have no relevant financial or non-financial interests to disclose. The study is financially supported by the Ministry of Education, Government of India.

References

1. Hoek, E.; Marinos, P.: Predicting tunnel squeezing problems in weak heterogeneous rock masses. Tunnels Tunn. Int. Part **1–2**, 1–20 (2000)
2. Majumder, D.; Viladkar, M.N.; Singh, M.: A multiple-graph technique for preliminary assessment of ground conditions for tunneling. Int. J. Rock Mech. Min. Sci. **100**, 278–286 (2017). https://doi.org/10.1016/j.ijrmms.2017.10.010
3. Singh, M.; Singh, B.; Choudhari, J.: Critical strain and squeezing of rock mass in tunnels. Tunn. Undergr. Sp. Technol. **22**, 343–350 (2007). https://doi.org/10.1016/j.tust.2006.06.005
4. Dwivedi, R.D.: Behaviour of Underground Excavations in Squeezing Ground Conditions. IIT Roorkee, London (2014)
5. Goel, R.K.; Jethwa, J.L.; Paithankar, A.G.: An empirical approach for predicting ground condition for runnelling and its practical benefits. In: University of Nevada (ed) The 35th U.S. Symposium on Rock Mechanics (USRMS), Reno, Nevada, pp. 431–35 (1995)
6. Goel, R.K.; Singh, B.: Engineering Rock Mass Classification: Tunnelling, Foundations and Landslides. Elsevier, London (2011)
7. Barton, N.: Some new Q-value correlations to assist in site characterisation and tunnel design. Int. J. Rock. Mech. Min. Sci. **39**, 185–216 (2002). https://doi.org/10.1016/S1365-1609(02)00011-4
8. Marinos, P.; Marinos, V.; Hoek, E.: Geological Strength Index (GSI): A characterization tool for assessing engineering properties for rock masses. In: Proceedings of the International Workshop on Rock Mass Classification in Underground Mining, pp. 13–21 (2007)
9. Saari, K.: Analysis of Plastic Deformation (Squeezing) of Layers Intersecting Tunnels and Shafts in Rock. University of California, Berkeley (1982)
10. Barla, G.; Bonini, M.; Debernardi, D.: Time dependent deformations in squeezing tunnels. In: The 12th International Conference of International Association for Computer Methods and Advances in Geomechanics (IACMAG), pp. 1–6 (2008)
11. Debernardi, D.; Barla, G.: New viscoplastic model for design analysis of tunnels in squeezing conditions. Rock Mech. Rock Eng. **42**, 259–288 (2009). https://doi.org/10.1007/s00603-009-0174-6
12. Aydan, O.; Akagi, T.; Kawamoto, T.: The squeezing potential of rocks around tunnels; theory and prediction. Rock Mech. Rock Eng. **26**, 137–163 (1993). https://doi.org/10.1007/BF01023620
13. Barla, G.; Debernardi, D.; Sterpi, D.: Time-dependent modeling of tunnels in squeezing conditions. Int. J. Geomech. ASCE **12**, 697–710 (2011). https://doi.org/10.1061/(ASCE)GM.1943-5622.0000163
14. Cantieni, L.; Anagnostou, G.: The interaction between yielding supports and squeezing ground. Tunn. Undergr. Sp. Technol. **24**, 309–322 (2009). https://doi.org/10.1016/j.tust.2008.10.001
15. Cui, L.; Zheng, J.J.; Zhang, R.J.; Dong, Y.K.: Elasto-plastic analysis of a circular opening in rock mass with confining stress-dependent strain-softening behaviour. Tunn. Undergr. Sp. Technol. **50**, 94–108 (2015). https://doi.org/10.1016/j.tust.2015.07.001
16. Hoek, E.; Brown, E.: Practical estimates of rock mass strength. Int. J. Rock Mech. Min. Sci. **34**, 1165–1186 (1997). https://doi.org/10.1016/S1365-1609(97)80069-X
17. Meguid, M.A.; Rowe, R.K.: Stability of D-shaped tunnels in a Mohr-Coulomb material under anisotropic stress conditions. Can. Geotech. J. **43**, 273–281 (2006). https://doi.org/10.1139/t06-004

18. Shalabi, F.I.; Al-Qablan, H.A.; Al-Hattamleh, O.H.: Elasto-plastic behavior of raghadan tunnel based on RMR and hoek-brown classifications. Geotech. Geol. Eng. **27**, 237–248 (2009). https://doi.org/10.1007/s10706-008-9225-0
19. Zhao, K.; Janutolo, M.; Barla, G.: A completely 3d model for the simulation of mechanized tunnel excavation. Rock Mech. Rock Eng. **45**, 475–497 (2012). https://doi.org/10.1007/s00603-012-0224-3
20. Hoek, E.; Carranza-torres, C.; Corkum, B.: Hoek-Brown failure criterion-2002 edition. In: Narms-Tac, pp. 267–273 (2002)
21. Hoek, E.; Brown, E.T.: Empirical strength criterion for rock masses. J. Geotech. Eng. Div. **106**, 1013–1035 (1980)
22. Sterpi, D.; Gioda, G.: Visco-Plastic behaviour around advancing tunnels in squeezing rock. Rock Mech. Rock Eng. **42**, 319–339 (2009). https://doi.org/10.1007/s00603-007-0137-8
23. Roateşi, S.: Finite element analysis of effect of lining on damage in viscoplastic rocks. Comput. Geotech. **49**, 1–6 (2013). https://doi.org/10.1016/j.compgeo.2012.10.001
24. Pan, X.D.; Hudson, J.A.: Plane strain analysis in modelling three-dimensional tunnel excavations. Int. J. Rock Mech. Min. Sci. Geomech. Abstr. **25**, 331–337 (1988). https://doi.org/10.1016/0148-9062(88)90010-1
25. Pan, X.D.; Hudson, J.A.; Cassie, J.: Large deformation of weak rocks at depth-a numerical case study. Rock Gt. Depth **5**, 613–620 (1989)
26. Eberhardt, E.: The Hoek-Brown failure criterion. Rock Mech. Rock Eng. **45**, 981–988 (2012). https://doi.org/10.1007/s00603-012-0276-4
27. Wan, R.G.: Implicit integration algorithm for Hoek-Brown elastic-plastic model. Comput. Geotech. **14**, 149–177 (1992). https://doi.org/10.1016/0266-352X(92)90031-N
28. Merifield, R.S.; Lyamin, A.V.; Sloan, S.W.: Limit analysis solutions for the bearing capacity of rock masses using the generalised Hoek-Brown criterion. Int. J. Rock Mech. Min. Sci. **43**, 920–937 (2006). https://doi.org/10.1016/j.ijrmms.2006.02.001
29. Basarir, H.; Ozsan, A.; Karakus, M.: Analysis of support requirements for a shallow diversion tunnel at Guledar dam site, Turkey. Eng. Geol. **81**, 131–145 (2005). https://doi.org/10.1016/j.enggeo.2005.07.010
30. Özsan, A.; Başarir, H.: Support capacity estimation of a diversion tunnel in weak rock. Eng. Geol. **68**, 319–331 (2003)
31. Gurocak, Z.; Solanki, P.; Zaman, M.M.: Empirical and numerical analyses of support requirements for a diversion tunnel at the Boztepe dam site, eastern Turkey. Eng. Geol. **91**, 194–208 (2007). https://doi.org/10.1016/j.enggeo.2007.01.010
32. Bagheri, B.; Soltani, F.; Mohammadi, H.: Prediction of plastic zone size around circular tunnels in non-hydrostatic stress field. Int. J. Min. Sci. Technol. **24**, 81–85 (2014). https://doi.org/10.1016/j.ijmst.2013.12.014
33. Choi, S.O.; Deb, D.: Supplementation of generalized hoek-brown yield surface through the singularity adjustment in elastic-plastic analysis. Geosyst. Eng. **8**, 43–50 (2005). https://doi.org/10.1080/12269328.2005.10541235
34. Owen, D.R.J.; Hinton, E.: Finite Elements Plasticity: Theory and Practice. Pineridge Press Limited, Swansea (1980)
35. Crisfield, M.A.: Nonlinear Finite Element Analysis of Solids and Structures, Vol. 2. Wiley, West Sussex (1996)
36. Zhang, Y.; Li, X.: Finite element analysis of the stability of tunnel surrounding rock with weak rock layer. Mod. Appl. Sci. **3**, 22–27 (2009)
37. Clausen, J.C.: Efficient Non-Linear Finite Element Implementation of Elasto-Plasticity for Geotechnical Problems. Aalborg University, Esbjerg Institute of Technology, Niels Bohrs Vej, Esbjerg, Denmark, vol. 8, pp. 6700 (2007)
38. Suchowerska, A.M.; Merifield, R.S.; Carter, J.P.; Clausen, J.: Prediction of underground cavity roof collapse using the Hoek-Brown failure criterion. Comput. Geotech. **44**, 93–103 (2012). https://doi.org/10.1016/j.compgeo.2012.03.014
39. Kumar, J.; Mohapatra, D.: Lower-bound finite elements limit analysis for Hoek-Brown materials using semidefinite programming. J. Eng. Mech. **143**, 04017077 (2017). https://doi.org/10.1061/(ASCE)EM.1943-7889.0001296
40. Karaoulanis, F.E.: Implicit numerical integration of nonsmooth multisurface yield criteria in the principal stress space. Arch. Comput. Methods Eng. **20**, 263–308 (2013). https://doi.org/10.1007/s11831-013-9087-3
41. Karaoulanis, F.E.; Chatzigogos, T.: Implicit numerical integration of the Hoek-Brown yield criterion in principal stress space. In: Fourth European Conference on Computational Mechanics, pp. 1–8. France, Paris (2010)
42. Modlhammer, H.M.: Numerical Methods for Tunneling Using Abaqus and Investigation of Long-Time-Effects of the Shotcrete Shell and its Impact on the Combined Support System. Montan University Leoben (2011)
43. Chortis, F.; Kavvadas, M.: Three-dimensional numerical analyses of perpendicular tunnel intersections. Geotech. Geol. Eng. (2020). https://doi.org/10.1007/s10706-020-01587-w
44. Wu, G.; Chen, W.; Rong, C., et al.: Elastoplastic damage evolution constitutive model of saturated rock with respect to volumetric strain in rock and its engineering application. Tunn. Undergr. Sp. Technol. **97**, 103284 (2020). https://doi.org/10.1016/j.tust.2020.103284
45. Clausen, J.; Damkilde, L.: An exact implementation of the Hoek-Brown criterion for elasto-plastic finite element calculations. Int. J. Rock. Mech. Min. Sci. **45**, 831–847 (2008). https://doi.org/10.1016/j.ijrmms.2007.10.004
46. Jin, A.; Wang, B.; Zhao, Y., et al.: Analysis of the deformation and fracture of underground mine roadway by joint rock mass numerical model. Arab. J. Geosci. **12**, 1–8 (2019). https://doi.org/10.1007/s12517-019-4741-1
47. Kalos, A.; Kavvadas, M.: A constitutive model for strain-controlled Strength Degradation of Rockmasses (SDR). Rock Mech. Rock Eng. **50**, 2973–2984 (2017). https://doi.org/10.1007/s00603-017-1288-x
48. Zhong, Z.; Wang, Z.; Zhao, M.; Du, X.: Structural damage assessment of mountain tunnels in fault fracture zone subjected to multiple strike-slip fault movement. Tunn. Undergr. Sp. Technol. **104**, 103527 (2020). https://doi.org/10.1016/j.tust.2020.103527
49. Dhawan, K.R.; Singh, D.N.; Gupta, I.D.: Three-dimensional finite element analysis of underground caverns. Int. J. Geomech. ASCE **4**, 224–228 (2004). https://doi.org/10.1061/?ASCE?1532-3641?2004?4:3?224?CE
50. Goel, R.K.; Jethwa, J.L.; Paithankar, A.G.: Tunnelling through the young Himalayas-a case history of the Maneri-Uttarkashi power tunnel. Eng. Geol. **39**, 31–44 (1995). https://doi.org/10.1016/0013-7952(94)00002-J
51. Balagurusamy, E.: Numerical Methods, 1st edn. Mc Graw Hill, London (1999)
52. Dassault Systems Simulia Corporation (2014) ABAQUS documentation and theory manual
53. Johnson, G.R.: A constitutive model and data for materials subjected to large strains. In: Proceedings of 7th Information of Symposium on Ballistics. The Hague, Netherlands (1983)
54. Lubliner, J.; Oliver, J.; Oller, S.; Oñate, E.: A plastic-damage model for concrete. Int. J. Solids Struct. **25**, 299–326 (1989). https://doi.org/10.1016/0020-7683(89)90050-4
55. IS 456 (2000) Concrete, Plain and Reinforced Concrete-Code of Practice, Tenth Report. New Delhi
56. Viladkar, M.N.: Geomechanical challenges: Practices and innovations. Indian Geotech. J. **48**, 1–51 (2018). https://doi.org/10.1007/s40098-017-0285-z

57. Majumder, D.: Response of Tunnels in Squeezing Ground Contitions. IIT Roorkee, New York (2021)
58. NAVFAC standards: Table of Ultimate Friction Factors for Dissimilar Materials. In: Civil Engineering Software https://www.finesoftware.eu/help/geo5/en/table-of-ultimate-friction-factors-for-dissimilar-materials-01/ (2019). Accessed 1 Jan 2020
59. Baltay, P.; Gjelsvik, A.: Coefficient of friction for steel on concrete at high normal stress. J Mater. Civ. Eng. **2**, 46–49 (1990)
60. Sharan, S.K.: Exact and approximate solutions for displacements around circular openings in elastic-brittle-plastic Hoek-Brown rock. Int. J. Rock Mech. Min. Sci. **42**, 542–549 (2005). https://doi.org/10.1016/j.ijrmms.2005.03.019
61. Carranza-Torres, C.; Fairhurst, C.: Application of the Convergence-Confinement Method of tunnel design to rock masses that satisfy the Hoek-Brown failure criterion. Tunn. Undergr. Sp. Technol. **15**, 187–213 (2000). https://doi.org/10.1016/S0886-7798(00)00046-8
62. Wang, H.N.; Utili, S.; Jiang, M.J.: An analytical approach for the sequential excavation of axisymmetric lined tunnels in viscoelastic rock. Int. J. Rock Mech. Min. Sci. **68**, 85–106 (2014). https://doi.org/10.1016/j.ijrmms.2014.02.002
63. Abaqus documentation-MIT: Abaqus documentation-MIT. In: abaqus-docs.mit.edu. https://abaqus-docs.mit.edu/2017/English/SIMACAEEXCRefMap/simaexc-c-docproc.htm (2017). Accessed 2 Feb 2020
64. Jain, M.S.; Jaitly, G.S.; Rajagopalan, G.S.N.S.: Geotechnical note on the alternative alignments between Heena and Tiloth adits. Science **2**, 7789 (1976)
65. Carranza-Torres, C.: Elasto-plastic solution of tunnel problems using the generalized form of the Hoek-Brown failure criterion. Int. J. Rock Mech. Min. Sci. **41**, 1–11 (2004). https://doi.org/10.1016/j.ijrmms.2004.03.111
66. IS-800: General Construction in Steel - Code of Practice. New Delhi, India (2007)